C. Q. Trinh, S. C. Ellis, J. S. Lawrence, A. J. Horton, J. Bland-Hawthorn, S. G. Leon-Saval, J. Bryant, S. Case, M. Colless, W. Couch, K. Freeman, L. Gers, K. Glazebrook, R. Haynes, S. Lee, H.-G. Löhmannsröben, S. Miziarski, J. O'Byrne, W. Rambold, M. M. Roth, B. Schmidt, K. Shortridge, S. Smedley, C. G. Tinney, P. Xavier, J. Zheng, "GNOSIS: a novel near-infrared OH suppression unit at the AAT," Proc. SPIE 8446, Ground-based and Airborne Instrumentation for Astronomy IV, 84463J (24 September 2012); http://doi.org/10.1117/12.926483

GNOSIS: a novel near-infrared OH suppression unit at the AAT

C. Q. Trinh[a], S. C. Ellis[b,a], J. S. Lawrence[b], A. J. Horton[b], J. Bland-Hawthorn[a,c], S. G. Leon-Saval[c], J. Bryant[a,d], S. Case[b], M. Colless[b], W. Couch[e], K. Freeman[f], L. Gers[b], K. Glazebrook[e], R. Haynes[g], S. Lee[b], H.-G. Löhmannsröben[h], S. Miziarski[b], J. O'Byrne[a], W. Rambold[g], M. M. Roth[g], B. Schmidt[f], K. Shortridge[b], S. Smedley[b], C. G. Tinney[i], P. Xavier[b], J. Zheng[b]

[a]Sydney Institute for Astronomy, School of Physics, The University of Sydney, NSW 2006, Australia;
[b]Australian Astronomical Observatory, PO Box 296, Epping, NSW 1710, Australia;
[c]Institute of Photonics and Optical Science, School of Physics, The University of Sydney, NSW 2006, Australia;
[d]ARC Centre for Excellence for All-sky Astrophysics (CAASTRO);
[e]Centre for Astrophysics and Supercomputing, Swinburne University of Technology, PO Box 218, Hawthorn, VIC 3122, Australia;
[f]Research School of Astronomy and Astrophysics, Australian National University, Cotter Rd., ACT, Canberra, Australia;
[g]innoFSPEC - Leibniz-Institut für Astrophysik Potsdam, An der Sternwarte 16, 14482 Potsdam, Germany;
[h]innoFSPEC - Institut für Chemie/Physikalische Chemie, Universität Potsdam, Karl-Liebknecht-Strasse 24-25, D-14472 Golm, Germany;
[i]Department of Astrophysics, School of Physics, University of NSW, NSW 2052, Australia

ABSTRACT

GNOSIS has provided the first on-telescope demonstration of a concept to utilize complex aperioidc fiber Bragg gratings to suppress the 103 brightest atmospheric hydroxyl emission doublets between 1.47–1.7 μm. The unit is designed to be used at the 3.9-meter Anglo-Australian Telescope (AAT) feeding the IRIS2 spectrograph. Unlike previous atmospheric suppression techniques GNOSIS suppresses the lines before dispersion. We present the results of laboratory and on-sky tests from instrument commissioning. These tests reveal excellent suppression performance by the gratings and high inter-notch throughput, which combine to produce high fidelity OH-free spectra.

Keywords: near-infrared, OH suppression, astrophotonics, fiber Bragg gratings, photonic lantern

1. INTRODUCTION

At near-infrared (NIR) wavelengths (0.9–1.8 μm) the bright and variable atmospheric emission, due mainly to the de-excitation of hydroxyl (OH) molecules,[1] makes ground-based spectroscopy at these wavelengths extremely challenging. Previous attempts to solve the NIR sky background problem include ultra-narrow band filters,[2] high dispersion masking,[3,4] and holographic filters.[5] However, none of these techniques achieve suppression over a broad wavelength range while maintaining high throughput, which is critical for a wide range of science cases.

OH suppression using aperiodic fiber Bragg gratings (FBGs)[6–8] achieves exactly this and is the closest we have come to a viable solution to the NIR sky background problem from the ground. GNOSIS is the first instrument to utilize FBG OH suppression technology. The aperiodic FBGs used in GNOSIS, made by Redfern

Send correspondence to c.trinh@physics.usyd.edu.au

Ground-based and Airborne Instrumentation for Astronomy IV, edited by Ian S. McLean, Suzanne K. Ramsay, Hideki Takami, Proc. of SPIE Vol. 8446, 84463J · © 2012 SPIE · CCC code: 0277-786X/12/$18 · doi: 10.1117/12.926483

Optical Components, are some of the most complex optical filters ever made. They contain around 50 narrow (≈ 0.2 nm) and irregularly-spaced notches over a span of ≈ 100 nm. Unlike printing multiple FBGs into a single fiber, these globally optimized gratings maintain high throughput between the notches. However, they can only be useful for OH suppression when printed in single-mode fibers (SMFs). Unfortunately, it is very difficult to couple light from a telescope into a SMF, which is the reason photonic lanterns are needed.

Photonic lanterns consist of a multi-mode fiber (MMF) connected to an SMF array by a taper transition which efficiently converts multi-mode (MM) light into single-mode (SM) light or vice versa.[9–11] The photonic lantern works by converting the excited modes in the MMF into the supermodes of the SMF array. GNOSIS uses photonic lanterns with 19 SMFs or "1×19" made by NKT Photonics. Attaching such photonic lanterns to an array of 19 FBGs yields a device with the light collecting ability of a MMF with the suppression performance of a SMF. Below we discuss the first on-telescope demonstration of this technology.

2. GRATING UNIT

The heart of GNOSIS is the grating unit where OH suppression is actually done. The grating unit contains 7 identical and independent branches housed within an aluminium enclosure, which is mounted to the instrument rack within the AAT Cassegrain cage. Each branch consists of an input 1×19 photonic lantern, 19 pairs of FBGs, and an output 19×1 photonic lantern all fusion spliced together. The field of view of each branch is small and we utilize 7 identical branches to cover more of the sky. However, this is at the expense of higher detector background because more spatial pixels are used to sample the object.

GNOSIS uses two FBGs in series to suppress sky lines over most of the H band (1.47–1.7 μm). Each device contains about 50 notches over a span of about 100 nm so two are necessary to cover the H band. The device covering the first and second halves of the H band referred to as H1 and H2, respectively. The notch positions, depths, and widths are based on the OH line positions and strengths from Rousselot et al.[12] Each FBG is packaged in an athermal stainless steel tube to prevent wavelength shifts due to strain and temperature variations.

Figure 1 shows the measured depths and widths of the H1 and H2 FBG notches. These were measured from the transmission spectra of the FBGs by fitting an $n = 5$ Butterworth profile to each notch. Figure 2 shows the measured throughput at several inter-notch wavelengths both in-band and out-of-band for both devices. These measurement were made using a cutback technique with a narrow tunable external cavity laser. The FBG performance is quite good. The notches are rather square, narrow (≈ 0.2 nm) and deep (≈ 25 dB) and the inter-notch throughput is high ($> 90\%$).

The 1×19 photonic lanterns consists of a 50 μm core diameter MMF (AFS50/125Y) connected to an array of 19 SMFs (SMF-28) by a taper with a ratio of 11 packaged in a steel case for mechanical protection. As mentioned before, the photonic lantern efficiently coverts MM to SM light by converting the excited modes in the MMF into the supermodes of the SMF array. The number of supermodes of the SMF array is equal to the number of SMFs. Thus, the loss in the photonic lanterns will be minimum when the number of excited modes in the MMF is matched to the number of SMFs. This constraints the focal ratio of the beam feeding the input photonic lantern. Table 1 lists the measured MM to SM loss of the input photonic lantern of each branch of the grating unit when fed with a f/5.8 beam or numerical aperture (NA) of 0.086. Also listed in Table 1 are the measured SM to MM loss for the output photonic lantern and the SM to MM NA of the input and output photonic lanterns of each branch of the grating unit.

The throughput of the grating unit as a whole was measured during installation by simulating illumination by the telescope with a 1550 nm superluminescent diode source. The average throughput of all 7 branches is $\approx 55\%$. The throughput as a function of wavelength was measured from dome lamp observations taken after installation with one branch set up to bypass the grating unit (control fiber). The difference in signal between the control fiber and the suppressed fibers is due mainly to the loss in the grating unit. Thus, taking the ratio of the control spectrum and one of the suppressed spectra and correcting for throughput variations in the other parts of the system gives the throughput as a function of wavelength for that particular grating unit branch. Figure 2 shows the throughput of grating unit branch 1. The notches appear as obvious dips in the throughput, but the resolution of IRIS2 makes them shallower and wider than indicated in Figure 1. The variation in the

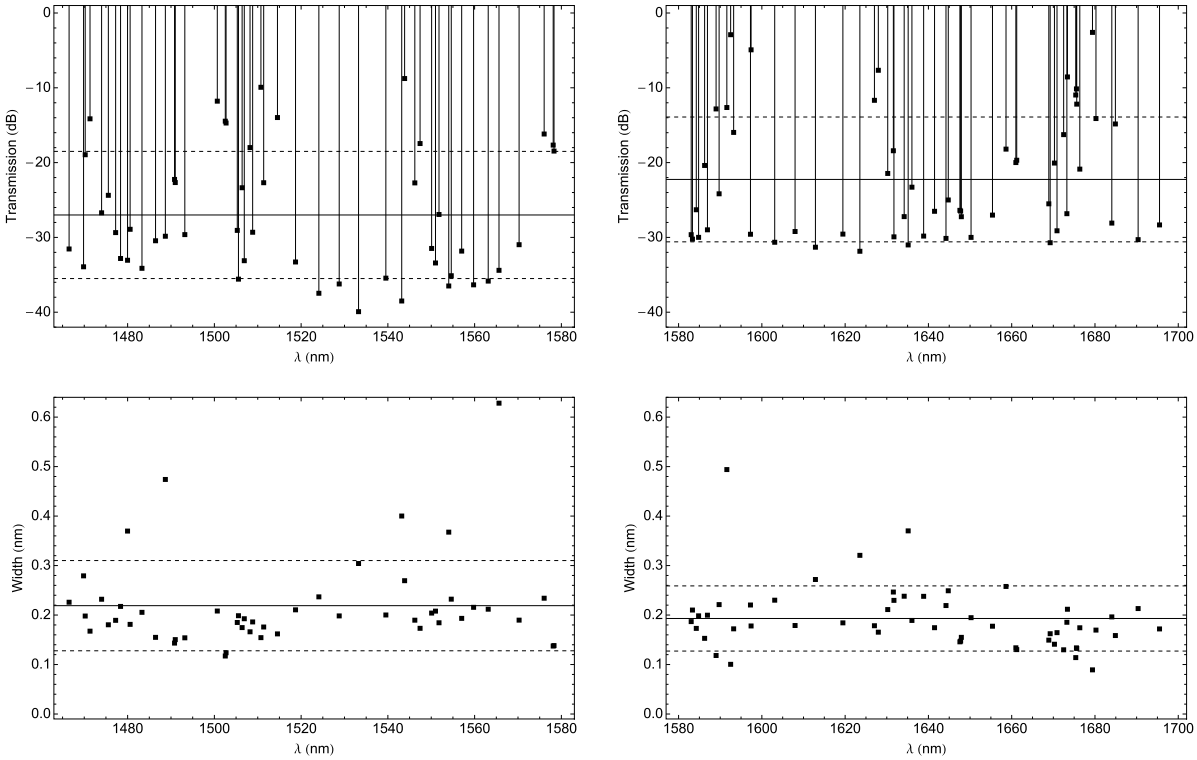

Figure 1. The measured notch depths (top) and widths (bottom) of the H1 (left) and H2 (right) FBGs. The solid and dashed horizontal lines show the mean and 1 σ range. The FBG notches are deep and narrow, which is ideal for OH suppression. Some notches are designed to be wider in order to suppressed several blended lines.

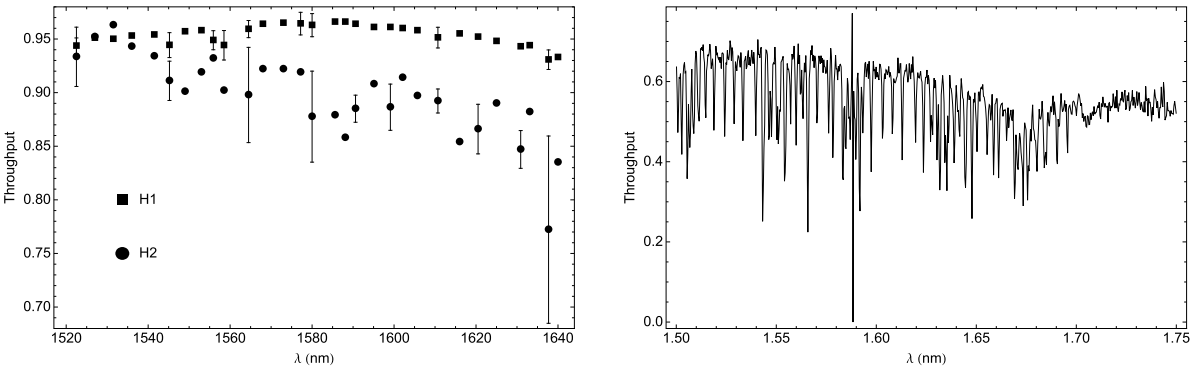

Figure 2. (Left) The measured throughput of the H1 (squares) and H2 (circles) FBGs at several inter-notch wavelengths both in-band and out-of-band. Points with error bars show the mean and 1 σ variation from several devices and points without error bars are measurements from a single device. The inter-notch throughput of the FBGs is high allowing the inter-notch regions to be efficiently used for science observations. (Right) The throughput of grating unit branch 1 measured with the IRIS2 spectrograph after system installation. The FBG notches are evident, but this spectrum does not reflect the true depth and width of the notches because of the low resolution of IRIS2. Comparing the two plots suggests that the main wavelength-independent loss in the grating unit comes from the photonic lanterns.

Table 1. Photonic lantern performance in each grating unit branch

Branch No.	Input		Output	
	MM to SM Loss	NA	SM to MM Loss	NA
1	0.67 dB	0.097	0.15 dB	0.101
2	0.71 dB	0.098	0.11 dB	0.107
3	0.77 dB	0.094	0.17 dB	0.106
4	N.A.	0.107	0.12 dB	0.105
5	0.64 dB	0.105	0.07 dB	0.101
6	0.71 dB	0.106	0.12 dB	0.105
7	N.A.	0.109	0.05 dB	0.095

inter-notch throughput with wavelength is due mainly to the increase in the linear loss of the fiber the FBGs are printed in at longer wavelengths. The wavelength-independent losses in the grating unit are due mainly to the photonic lanterns, specifically the MM to SM loss of the input lantern. By improving the performance of the photonic lanterns, we may in theory be able to obtain a grating unit with a throughput close to that of the individual FBGs.

3. FORE-OPTICS UNIT

The f/8 beam from the telescope is fed to the grating unit using a fore-optics unit mounted at the Cassegrain focus and a fiber bundle. The fore-optics unit contains an optical relay and a 7 element hexagonal lenslet (2 mm flat-to-flat) array integral field unit (IFU). When the beam exits the telescope, a mirror with a central aperture is used to pass the central region of the focal plane to the IFU while the rest of the beam is diverted to an acquisition camera. The IFU images the central ≈ 1 arcsec^2 region of the focal plane. Each IFU element feeds an $\approx$ f/6.5 beam into a 50 μm core diameter fiber that is fused to the MMF of one of the input photonic lanterns. We measured the throughput of the fore-optics unit (relay + IFU + fiber bundle) during assembly and during installation by illuminating the entrance aperture with an f/8 beam with a 1550 nm superluminescent diode source to simulate illumination by the telescope. The average throughput of all 7 channels is $\approx 76\%$.

4. IRIS2 INTERFACE UNIT

The OH suppressed light exiting the grating unit is transported to the IRIS2 spectrograph,[13] which is located on the dome floor underneath the telescope, by a second 50 μm core diameter fiber bundle 12 m in length. The fibers are terminated in a linear slit block within the IRIS2 interface unit assembly, which sits above the IRIS2 dewar window. An optical relay with a magnification of 3 within the interface unit images the fibers onto the IRIS2 slit plane, which is inside the instrument dewar. The $\approx$ f/5 beam from the fibers is converted into a $\approx$ f/15 beam to obtain a spectrograph resolution of $R \sim 2000$. This beam is well within the maximum acceptance cone of IRIS2 (f/8) and there is room for errors due to focal ratio degradation (FRD). Custom slit masks with 180 and 250 μm diameter holes and a f/12 coldstop are placed within IRIS2 to block extraneous light. We measured the throughput of the IRIS2 interface unit (fiber bundle + slit block + relay) during installation with the entrance aperture of the fore-optics unit illuminated by an f/8 beam from a 1550 nm superluminescent diode source as before. The average throughput of all 7 channels is $\approx 93\%$. The misalignment between the slit block and the slit mask holes results in an additional 5-10% loss.

5. DATA REDUCTION

GNOSIS was commissioned at the 3.9-meter Anglo-Australian Telescope at Siding Spring Observatory on five separate observing runs during March, May, July, September, and November of 2011. Observations were made with the H broadband filter, the f/12 coldstop, the slit mask with either 180 or 250 μm diameter holes, and the grism in multiple-read mode (MRM), where the 1024×1024 Rockwell Hawaii-1 detector is non-destructively read out during the exposure and the final image is a linear least-squares fit through all the reads. The read noise is

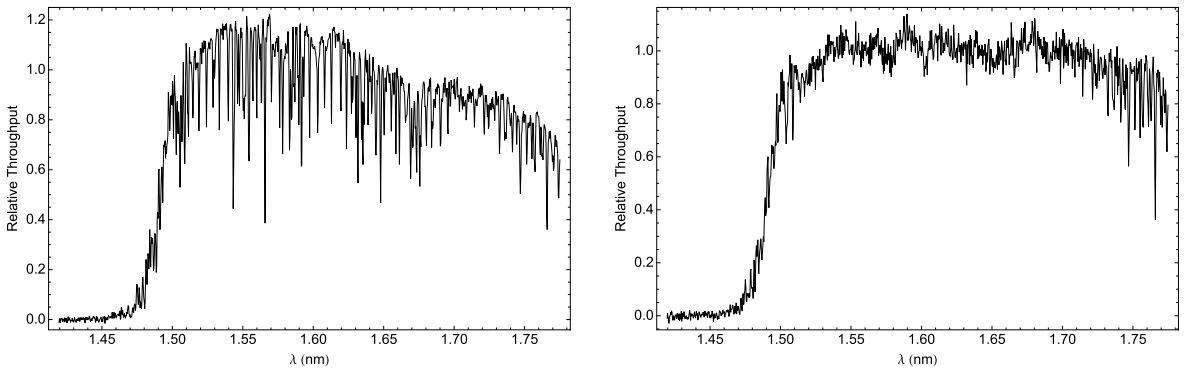

Figure 3. Instrument response for the suppressed fibers (left) and the control fiber (right). This was measured from an observation of HIP 114191 on 03 September 2011. The FBG notches appear in the suppressed fiber as significant drops in throughput but are shallower and wider than indicated in Figure 1 because of the resolution of IRIS2.

minimized for MRM observations (8 e^-). The detector dark current is ≈ 0.0015 e^- s^{-1}. The dark current and read noise can be significant sources of background due to the large number of spatial pixels used in GNOSIS observations. We measured the point spread function of GNOSIS with IRIS2 to be 2.0 pixels FWHM, which corresponds to a spectral resolution of $R \approx 2350$.

Each image is corrected for detector non-linearities before further processing. The spectrum in each fiber is extracted following the "Gaussian summation extraction by least squares" from Sharp & Birchall.[14]

The extracted spectrum of each fiber must be corrected for throughput variations in each branch. We measured the fiber-to-fiber variation from observations of dome flat fields. First, the dome flat spectrum in each fiber is extracted. Each spectrum is integrated and the value is normalized to the mean value over all 7 fibers. We correct object spectra by dividing by the fiber-to-fiber variation.

The spectrum in each fiber is wavelength calibrated using a xenon arc lamp observation. The arc spectra are extracted and we fit a cubic polynomial to the pixel position of each xenon line in each fiber. The wavelength solution for each fiber is accurate to ≈0.2 nm.

GNOSIS spectra are spread over two detector quadrants and the spectra must be corrected for inter-quandrant cross talk.[15] This is done by computing the median count rate at $\lambda < 1.47$ μm (the H filter cuts on at 1.5 μm and this region should have no counts) and subtracting it from the spectrum.

The final reduction we apply to all observations is an instrument response correction (relative throughput of the system as a function of wavelength). This is measured from an observation of an A0V standard star. The stellar spectra are extracted and reduced as described above. The sky-subtracted spectrum in each fiber is divded by a model spectrum of Vega[16] and normalized to the median value between 1.5–1.69 μm. Figure 3 shows the instrument response measured from an observation of HIP 114191 on 03 September 2011. To apply an instrument response correction, we divide the object spectrum by the instrument response function.

6. INSTRUMENT THROUGHPUT

Above, we have discussed the measurement of the throughput of each GNOSIS subsystem. Overall, the measured throughput of GNOSIS is ≈ 36%. On-sky, there are additional losses in throughput from the telescope (88%), relay alignment (95%), and IRIS2 (12%). Thus, the end-to-end throughput of the system is ≈ 4%, or ≈ 2% for a point source assuming typical aperture losses.

The observations of A0V standard stars may also be used to measure the end-to-end throughput of our system. The end-to-end throughput is measured in a similar fashion to the instrument response except the model spectrum of Vega is scaled to the appropriate brightness with an estimate for aperture losses. During the September commissioning, the I band seeing was measured to be ≈ 1.5 arcsec. Although the aperture losses

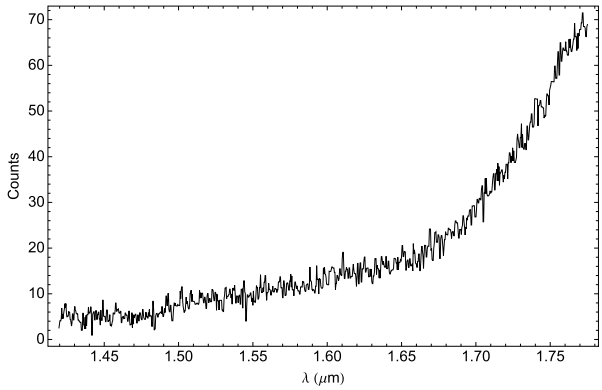

Figure 4. The spectrum in the central fiber of a 30 minute cold frame. This is used to remove the thermal background from our blank sky observations.

are uncertain, the A0V star observations taken during the September run are consistent with an end-to-end throughput of $\approx 2\%$ assuming typical apertures losses for the measured seeing.

7. SKY BACKGROUND

Here, we measure the suppression performance of GNOSIS. A total of 45 blank sky observations were taken during the September run at various locations on the sky. The exposure time of these observations were either 15 or 30 minutes. The instrument thermal background is significant in GNOSIS observations and a separate thermal background subtraction must be done for blank sky observations. This is accomplished by obtaining cold frames with same exposure time, where the fore-optics unit is pointed at a container of liquid nitrogen. In this configuration, the only signal reaching the detector should be the instrument thermal background and detector noise. Figure 4 shows the dark-subtracted cold frame spectrum from the central GNOSIS fiber. The counts at $\lambda < 1.47$ μm are non-zero because of inter-quadrant cross-talk (see below). Alternatively, we can fit a thermal blackbody spectrum to the continuum points in between the OH lines for $\lambda > 1.7$ μm and subtract the best fitting model from our spectrum.

Figure 5 shows the cold-subtracted blank sky spectrum from 6 suppressed fibers and the control fiber from 8.75 hr of observations from 1-4 September 2011 after Moonset and > 60 degrees from the Moon. The spectra are flux-calibrated assuming an efficiency of 3.3%. The strong suppression of the OH lines between 1.5–1.7 μm is evident. 78% of the OH lines were suppressed at the target suppression levels.

We compute the background reduction per pixel by taking the ratio of these two spectra and the result is shown in Figure 6. The reduction in the integrated background between 1.5–1.7 μm is ≈ 7.5. This is similar to the value reported by Ellis et al.[18] who analyzed a slightly different set of blank sky observations and utilized a best fitting model subtraction for the thermal background correction.

Although the suppression performance of GNOSIS is excellent, the reduction in the background between the OH lines is not at the level predicted by Ellis & Bland-Hawthorn.[17] There are several possibilities. First, there may be residual instrumental emission that was not properly removed in the data reduction. Second, an unaccounted for source may dominate the interline regions. Lastly, it is possible that the OH line model used to design the FBGs is inaccurate and some lines are not suppressed. A full discussion may be found in Ellis et al.[18] The prototype nature of GNOSIS and retrofitting it to IRIS2 results in increased thermal background and detector background, which makes it difficult to draw conclusions about the interline background. Nonetheless, the OH suppression is excellent and the high thermal and detector background is not intrinsic to FBG OH suppression systems and may be addressed in future systems.

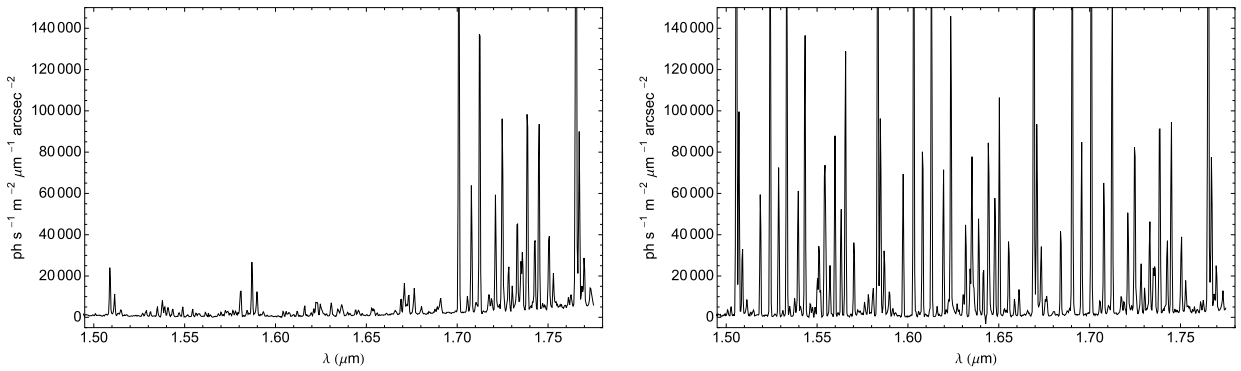

Figure 5. The cold-subtracted spectrum of blank sky with OH suppression (left) and without (right) from 8.75 hr of observations from 1-4 September 2011. The OH lines between 1.5–1.7 μm are strongly suppressed (78% are suppressed at or exceeding the target level).

8. INSTRUMENT SENSITIVITY

The sensitivity of GNOSIS is measured from an observation of a low surface brightness galaxy HIZOA J0836-43 (H band surface brightness of 17.3 mag arcsec^2) in order to circumvent the issue of unknown aperture losses. The sky-subtracted spectrum is divded by the square root of the non-subtracted spectrum to obtain the signal-to-noise per pixel. The median signal-to-noise per pixel is ≈ 10. The same analysis on the spectrum through the control fiber yields the same result, indicating that there is no improvement in signal-to-noise when using GNOSIS. This is because OH suppression mainly improves the signal-to-noise near the OH lines. In between the lines (the region that dominates the sensitivity calculation) there is no reduction in the background and the loss in throughput deteriorates the signal-to-noise. Low sensitivity is not inherent to FBG OH suppression systems and reducing the thermal and the detector background would significantly increase the system signal-to-noise in future systems.

9. SUMMARY

We have provided the first demonstration of the use of FBGs for OH suppression with the GNOSIS instrument. The instrument successfully suppressed most of the OH lines between 1.5–1.7 μm. In fact, 78% of the OH lines were suppressed at the target level or greater. Unfortunately, no reduction in the background between the lines was observed. Possible causes for this include residual instrumental emission, unaccounted for interline emission, and/or the FBGs are not suppressing the OH lines because of inaccuracies in the OH line model used to design the FBGs. The overall efficiency of the system was $\approx 4\%$, including telescope, GNOSIS, and IRIS2. The sensitivity of GNOSIS + IRIS2 is about the same as standard IRIS2 observations due to the low overall throughput of the system, the increase in thermal background from the IRIS2 interface unit, and the higher detector background from the small FOV of each fiber. These deficiencies are not inherent to OH suppression systems and we are currently working on new designs that will boost throughput and sensitivity and complement the excellent suppression performance.

GNOSIS itself has a throughput of $\approx 36\%$. The grating unit has the lowest throughput of the three GNOSIS subsystems. The throughput and FOV of each fiber may be increased significantly in the near future using FBGs in multi-core fibers (MCFs) with the ends tapered down into a MMF.[19] These MCFs typically have about 120 cores within a 230 μm cladding. They would reduce the loss in the photonic lanterns that comes from a mismatch between the excited modes in the MMF and the supermodes in the SMF array, no fusion splices would be required, and the size of the grating unit would be reduced to a small fiber. It would also allow the grating unit to be fed with a much faster beam ($\approx$ f/2.3), which would increase the fiber's FOV to ≈ 1.2 arcsec and significantly increase the signal-to-noise. Our group is currently working to implement MCFBGs for future OH suppression instruments.[20]

Retrofitting GNOSIS to the existing IRIS2 spectrograph resulted in higher thermal background and additional loss in throughput, both of which degrades the instrument sensitivity. Additionally, the IRIS2 detector noise characteristics makes it difficult to draw conclusions regarding the interline background because we are in the regime of very low counts where such systematic errors are very significant. We are currently designing a high efficieny low background spectrograph optimized for a fiber feed, called PRAXIS.[21] It will include a fiber vacuum feed through and a detector with low intrinsic noise, such as a Hawaii-2RG. Such a spectrograph will eliminate the need for a spectrograph interface unit, which will help reduce the instrument thermal background and improve throughput.

The increased sensitivity and low noise characteristics from these improvements will allow us to determine if we have indeed reached a floor in the interline continuum. This may be the case given that the absolute level of the interline continuum measured by GNOSIS using a best fitting model for the thermal background correction, $\approx$ 900 photon s^{-1} m^{-2} $arcsec^{-2}$ μm^{-1}, is similar to previous measurements.[22,23] If unsuppressed lines due to inaccuracies in the OH line models used design the FBGs are responsible for the interline continuum floor, the FBGs may be re-designed using a more accurate line model. Even if a significant reduction in the interline background is not found, FBG OH suppression will still provide benefits at low resolutions (500< R <3000).[18] Previously, observations at these resolutions were too low to resolve out the OH lines and the interline regions were useless for science. This is no the case with FBG OH suppression.

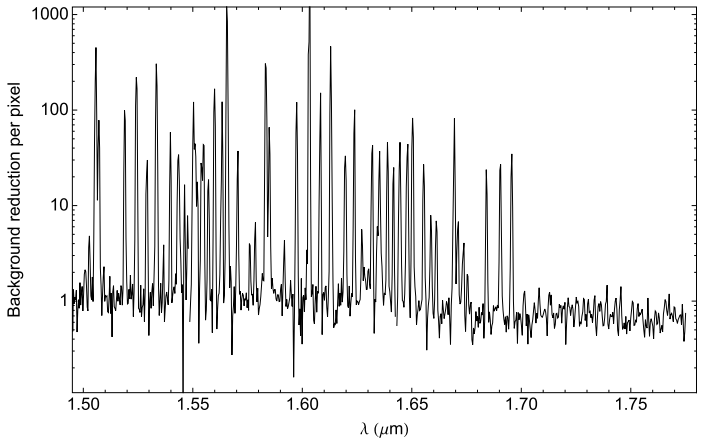

Figure 6. The background reduction per pixel computed from the spectra in Figure 5. The suppression near the OH lines is very strong, but the significant reduction between the lines predicted by Ellis and Bland-Hawthorn[17] is not seen. The lack of reduction may be from residual instrumental emission, an unaccounted for continuum source and/or unsuppressed lines. The prototype nature of GNOSIS and retrofitting it to IRIS2 resulted in increased thermal background and detector background, which makes it difficult to draw conclusions about the interline background.

REFERENCES

[1] I. A. B. Meinel, "OH Emission Bands in the Spectrum of the Night Sky", *ApJ* **111**, p. 555, 1950.

[2] A. Horton, I. Parry, J. Bland-Hawthorn, S. Cianci, D. King, R. McMahon, and S. Medlen, "DAzLE: the dark ages z (redshift) Lyman-α Explorer", *Proc. SPIE* **5492**, p. 1022, 2004.

[3] F. Iwamuro, K. Motohara, T. Maihara, R. Hata, and T. Harashima, "OHS: OH-Airglow Suppressor for the Subaru Telescope", *Proc. Astr. Soc. Japan* **53**, p. 355, 2001.

[4] K. Motohara, F. Iwamuro, T. Maihara, S. Oya, H. Tsukamoto, M. Imanishi, H. Terada, M. Goto, J. Iwai, H. Tanabe, R. Hata, T. Taguchi, and T. Harashima, "CISCO: Cooled Infrared Spectrograph and Camera for OHS on the Subaru Telescope", *Proc. Astr. Soc. Japan* **54**, p. 315, 2002.

[5] S. Blais-Ouellette, E. Artigau, F. Havermeyer, K. Matthews, C. Moser, D. Psaltis, and G. J. Steckman, "Multi-notch holographic filters for atmospheric lines suppression", *Proc. SPIE* **5494**, p. 554, 2004.

[6] J. Bland-Hawthorn, M. Englund, and G. Edvell, "New approach to atmospheric OH suppression using an aperiodic fiber Bragg grating", *Optics Express* **12**, p. 5902, 2004.
[7] J. Bland-Hawthorn, A. Buryak, and K. Kolossovski, "Optimization algorithm for ultrabroadband multichannel aperiodic fiber Bragg grating filters", *J. O. S. A.* **25**, p. 153, 2008.
[8] J. Bland-Hawthorn, S. C. Ellis, S. G. Leon-Saval, R. Haynes, M. M. Roth, H. -G. Löhmannsröben, A. J. Horton, J. -G. Cuby, T. A. Birks, J. S. Lawrence, P. Gillingham, S. D. Ryder, and C. Trinh, "A complex multi-notch astronomical filter to suppress the bright infrared sky", *Nature Communications* **2**, pp. 581, 2011.
[9] S. G. Leon-Saval, T. Birks, J. Bland-Hawthorn, and M. Englund, "Multimode fiber devices with single-mode performance", *Optics Letters* **30**, p. 19, 2005.
[10] D. Noordegraaf, P. M. Skovgaard, M. D. Nielsen, and J. Bland-Hawthorn, "Efficient multi-mode to single-mode coupling in a photonic lantern", *Optics Express* **17**, p. 1988, 2009.
[11] S. G. Leon-Saval, A. Argyros, and J. Bland-Hawthorn, "Photonic lanterns: a study of light propagation in multimode to single-mode converters", *Optics Express* **18**, pp. 8430–8439, 2010.
[12] P. Rousselot, C. Lidman, J. -G. Cuby, G. Moreels, and G. Monnet, "Night-sky spectral atlas of OH emission lines in the near-infrared", *A&A* **354**, pp. 1134–1150, 2000.
[13] C. G. Tinney, S. D. Ryder, S. C. Ellis, V. C. Churilov, J. Dawson, G. A. Smith, L. Waller, J. D. Whittard, R. Haynes, A. Lankshear, J. R. Barton, C. J. Evans, K. Shortridge, T. Farrell, and J. Bailey, "IRIS2: a working infrared multi-object spectrograph and camera", *Proc. SPIE* **5492**, p. 998, 2004.
[14] R. Sharp and M. N. Birchall, "Optimal Extraction of Fibre Optic Spectroscopy", *PASA* **27**, pp. 91–103, 2010.
[15] C. G. Tinney, A. J. Burgasser, and J. .D Kirkpatrick, "Infrared Parallaxes for Methane T Dwarfs", *AJ* **126**, pp. 975–992, 2003.
[16] F. Castelli and R. L. Kurucz, "Model atmospheres for VEGA", *A&A* **28**, pp. 817–834, 1994.
[17] S. C. Ellis and J. Bland-Hawthorn, "The case for OH suppression at near-infrared wavelengths", *MNRAS* **386**, p. 47, 2008.
[18] S. C. Ellis, J. Bland-Hawthorn, J. Lawrence, A. J. Horton, C. Trinh, S. G. Leon-Saval, K. Shortridge, J. Bryant, S. Case, M. Colless, W. Couch, K. Freeman, L. Gers, K. Glazebrook, R. Haynes, S. Lee, H. -G. Löhmannsröben, J. O'Byrne, S. Miziarski, M. Roth, B. Schmidt, C. G. Tinney, and J. Zheng, "Suppression of the near-infrared OH night sky lines with fibre Bragg gratings–first results", *MNRAS*, submitted.
[19] T. Birks, A. Diez, J. L. Cruz, S. G. Leon-Saval, and D. F. Murphy, "Fibers are Looking Up: Optical Fiber Transition Structures in Astrophotonics", Frontiers in Optics, 2010.
[20] S. Min, C. Trinh, S. G. Leon-Saval, N. Jovanovic, P. R. Gillingham, J. Bland-Hawthorn, J. S. Lawrence, T. A. Birks, M. M. Roth, R. Haynes, L. Fogarty, "Multicore fibre Bragg grating developments for OH suppression", Proc. SPIE, 8450-131, 2012.
[21] A. J. Horton, S. C. Ellis, J. S. Lawrence, and J. Bland-Hawthorn, "PRAXIS: a low background NIR spectrograph for fibre Bragg grating OH suppression", Proc. SPIE, 8450-65, 2012.
[22] T. Maihara, F. Iwamuro, T. Yamashita, D. N. B. Hall, L. L. Cowie, A. T. Tokunaga, and A. Pickles, "Observations of the OH airglow emission", *PASP* **105**, pp. 940–944, 1993.
[23] J. Cuby, C. Lidman, and C. Moutou, "ISSAC: 18 Months of Paranal Science Operations", *ESO Messenger* **101**, pp. 2–8, 2000.